A numerical investigation of the effect of vertex geometry on localized surface plasmon resonance of nanostructures

W. Y. Ma,[1] H. Yang,[1] J. P. Hilton,[2] Q. Lin,[2] J. Y. Liu[1], L. X. Huang,[1] and J. Yao[1,*]

[1]*State Key Lab of Optical Technologies for Microfabrication, Institute of Optics and Electronics, Chinese Academy of Science, Chengdu, 610209, China*

[2]*Department of Mechanical Engineering, Columbia University, New York, NY 10027, USA*

**junyao@ioe.ac.cn*

Abstract: Advances in nanofabrication and nano-scale measurement methods now allow for fabrication of highly detailed nanometer-scale topographic features. As geometric features greatly impact the formation of an electromagnetic field in response to incident light, this in turn calls for the study of the effects of new features of nanostructures on their performance in applications such as localized surface plasmon resonance (LSPR) sensing. This paper studies the effects of vertex features of a single nanostructure on its LSPR properties. A general relationship between the LSPR spectra and the vertex features of a nanoparticle is established. The results of electrodynamics calculations show that a delta-star with a relatively small vertex angle exhibits a bigger resonant wavelength than one with a large vertex angle. Moreover, the sensing performance initially increases, and then decreases as angular size of the vertices increases, with a turning point of 30°. It is also shown that for nanostars with different numbers of vertices, the resonant wavelength undergoes a blue shift and the sensing performance grows poorer as the number of vertices increases. A regular vertex angle of 30° displays the greatest figure of merit (*FOM*) value for LSPR applications, approximately 9.5 RIU^{-1}.

OCIS codes: (240.6680) surface plasmons; (260.3910) Metal optics; (280.4788) Optical sensing and sensors.

References and Links

1. T. Kalkbrenner, U. Hkanson, and V. Sandoghdar, "Tomographic plasmon spectroscopy of a single gold nanoparticle," Nano Lett. **4**(12), 2309–2314 (2004).
2. H. J. Huang, C. P. Yu, H. C. Chang, K. P. Chiu, H. Ming Chen, R. S. Liu, and D. P. Tsai, "Plasmonic optical properties of a single gold nano-rod," Opt. Express **15**(12), 7132–7139 (2007).
3. J. M. McMahon, Y. Wang, L. J. Sherry, R. P. Van Duyne, L. D. Marks, S. K. Gray, and G. C. Schatz, "Correlating the structure, optical spectra, and electrodynamics of single silver nanocubes," J. Phys. Chem. C **113**, 2731–2735 (2009).
4. K. A. Willets, and R. P. Van Duyne, "Localized surface plasmon spectroscopy and sensing," Annu. Rev. Chem. **58**(1), 267–297 (2007).
5. K. J. Lee, P. D. Nallathamby, L. M. Browning, C. J. Osgood, and X. H. N. Xu, "In vivo imaging of transport and biocompatibility of single silver nanoparticles in early development of zebrafish embryos," ACS Nano **1**(2), 133–143 (2007).
6. D. Lasne, G. A. Blab, S. Berciaud, M. Heine, L. Groc, D. Choquet, L. Cognet, and B. Lounis, "Single nanoparticle photothermal tracking (SNaPT) of 5-nm gold beads in live cells," Biophys. J. **91**(12), 4598–4604 (2006).
7. A. D. McFarland, and R. P. Van Duyne, "Single silver nanoparticles as real-time optical sensors with zeptomole sensitivity," Nano Lett. **3**(8), 1057–1062 (2003).
8. J. N. Anker, W. P. Hall, O. Lyandres, N. C. Shah, J. Zhao, and R. P. Van Duyne, "Biosensing with plasmonic nanosensors," Nat. Mater. **7**(6), 442–453 (2008).
9. S. Kim, J. Jin, Y. J. Kim, I. Y. Park, Y. Kim, and S. W. Kim, "High-harmonic generation by resonant plasmon field enhancement," Nature **453**(7196), 757–760 (2008).

#118796 - $15.00 USD Received 26 Oct 2009; revised 3 Dec 2009; accepted 6 Dec 2009; published 6 Jan 2010

10. J. J. Mock, D. R. Smith, and S. Schultz, "Local refractive index dependence of plasmon resonance spectra from individual nanoparticles," Nano Lett. **3**(4), 485–491 (2003).
11. W. Y. Ma, J. Yao, H. Yang, J. Y. Liu, F. Li, J. P. Hilton, and Q. Lin, "Effects of vertex truncation of polyhedral nanostructures on localized surface plasmon resonance," Opt. Express **17**(17), 14967–14976 (2009).
12. K. Ueno, S. Juodkazis, V. Mizeikis, D. Ohnishi, K. Sasaki, and H. Misawa, "Inhibition of multipolar plasmon excitation in periodic chains of gold nanoblocks," Opt. Express **15**(25), 16527–16539 (2007).
13. K. H. Su, Q. H. Wei, and X. Zhang, "Tunable and augmented plasmon resonances of Au/SiO2/Au nanodisks," Appl. Phys. Lett. **88**(063118), 1–3 (2006).
14. B. Sepúlveda, Y. Alaverdyan, J. Alegret, M. Käll, and P. Johansson, "Shape effects in the localized surface plasmon resonance of single nanoholes in thin metal films," Opt. Express **16**(8), 5609–5616 (2008).
15. K. L. Kelly, E. Coronado, L. L. Zhao, and G. C. Schatz, "The optical properties of metal nanoparticles: the Influence of size, shape, and dielectric environment," J. Phys. Chem. B **107**(3), 668–677 (2003).
16. J. P. Kottmann, O. J. F. Martin, D. R. Smith, and S. Schultz, "Dramatic localized electromagnetic enhancement in plasmon resonant nanowires," Chem. Phys. Lett. **341**(1-2), 1–6 (2001).
17. G. C. Schatz, and R. P. Van Duyne, "Electromagnetic mechanism of surface-enhanced spectroscopy," in *Handbook of vibrational Spectroscopy*, J. M. Chalmers and P. R. Griffiths, Ed., New York, Wiley, 759–774 (2002).
18. L. J. Sherry, R. Jin, C. A. Mirkin, G. C. Schatz, and R. P. Van Duyne, "Localized surface plasmon resonance spectroscopy of single silver triangular nanoprisms," Nano Lett. **6**(9), 2060–2065 (2006).
19. L. J. Sherry, S. Chang, G. C. Schatz, and R. P. Van Duyne, "Localized surface plasmon resonance spectroscopy of single silver nanocubes," Nano Lett. **0**(0): A-E (2005)
20. S. Yin, Q. Deng, X. Luo, C. Du, and Y. Zhang, "The coupled electric field effects on localized surface plasmon resonance in nanoparticle arrays," J. Appl. Phys. **104**, 1–5 (2008).
21. J. P. Kottmann, and O. J. F. Martin, "Plasmon resonant coupling in metallic nanowires," Opt. Express **8**(12), 655–663 (2001).
22. S. Zou, and G. C. Schatz, "Coupled plasmonic plasmon/photonic resonance effects in SERS," in Surface-Enhanced Raman Scattering – Physics and Applications, Topics Appl. Phys., K. Kneipp, M. Moskovits, H. Kneipp, Eds. Berlin, Springer, **103**, 67–87 (2006).
23. J. Sung, E. M. Hicks, R. P. Van Duyne, and K. G. Spears, "Nanoparticle spectroscopy: plasmon coupling in finite-size two-dimensional arrays of cylindrical silver nanoparticles," J. Phys. Chem. C **112**(11), 4091–4096 (2008).
24. C. L. Nehl, H. Liao, and J. H. Hafner, "Optical Properties of Star-Shaped Gold Nanoparticles," Nano Lett. **6**(4), 683–688 (2006).
25. G. Mie, "Contributions to the optics of turbid media, particularly of colloidal metal solutions," Annalen der Physik **25**, 377–445 (1908).
26. R. Gans, "The form of ultramicroscopic gold particles," Ann. Phys. **37**(5), 881–900 (1912).
27. R. Gans, "Form of ultramicroscopic particles of silver," Ann. Phys. **47**(10), 270–284 (1915).
28. A. Taflove, and S. Hagness, *Computational Electrodynamics: the Finite-Difference Time-Domain Method*, (Arthech House, 2000).
29. FDTD lumerical online help: www.lumerical.com.
30. K. S. Yee, "Numerical solution of initial boundary value problems involving maxwell's equations in isotropic media," IEEE Trans. Antenn. Propag. **14**(3), 302–307 (1966).
31. E. D. Palik, *Handbook of optical constants of solids III*, (Academic Press, 1998).
32. M. M. Miller, and A. A. Lazarides, "Sensitivity of metal nanoparticle surface plasmon resonance to the dielectric environment," J. Phys. Chem. B **109**(46), 21556–21565 (2005).
33. C. L. Haynes, A. D. McFarland, L. Zhao, R. P. Van Duyne, G. C. Schatz, L. Gunnarsson, J. Prikulis, B. Kasemo, and M. Käll, "Nanoparticle optics: the importance of radiative dipole coupling in two-dimensional nanoparticle arrays," J. Phys. Chem. B **107**(30), 7337–7342 (2003).
34. J. Sung, E. M. Hicks, R. P. Van Duyne, and K. G. Spears, "Nanoparticle spectroscopy: plasmon coupling in finite-size two-dimensional arrays of cylindrical silver nanoparticles," J. Phys. Chem. C **112**(11), 4091–4096 (2008).

1. Introduction

Studies of single metal nanoparticles (SMNPs) have attracted growing interest in the past decade due to their advantages over large ensembles of particles [1,2], including enhanced optical characteristics and sensing abilities. In LSPR, a SMNP absorbs and scatters light, resulting in an extinction spectrum (also called an LSPR spectrum) that can be detected by dark-field microscopy [3,4]. The LSPR spectrum is sensitive to the dielectric properties of the medium and a SMNP could potentially serve as an independent sensor [5–7]. SMNP sensors in multiplex assays offer narrower bandwidth, improved absolute detection limits, and higher spatial resolution than fixed arrays of SMNPs [8]. Due to these characteristics, SMNPs have advantages for use in immunoassays and other biochemical sensing measurements in solution or inside tissues where fixed arrays are not accessible.

#118796 - $15.00 USD Received 26 Oct 2009; revised 3 Dec 2009; accepted 6 Dec 2009; published 6 Jan 2010

In recent years, some new synthesis and nanofabrication methods, such as electron beam lithography (EBL) and focused ion beam (FIB) lithography have been developed to fabricate large ensembles of metal nanoparticles and SMNPs with specific topographic features [9–11], which can reveal aspects of underlying scientific principles and produce designs tailored for specific applications via control of the nano-scale geometry. Periodic chains of gold nanoblocks have been fabricated which can sustain dipolar localized plasmon modes similar to those of smooth nanorods [12]. Recent work by Xiang Zhang and associates has developed a new kind of nanodisk employing multiple layers of metal [13], which exhibits high scattering intensity to be applied in surface enhanced Raman scattering (SERS). In addition, microscopy methods such as atomic force microscopy (AFM), scanning electron microscopy (SEM) and transmission electron microscopy (TEM) are effective complementary tools in the characterization of SMNP samples, providing methods for examination of nanoscale geometries and morphologies. These advances have renewed interest in the optical properties and sensing performance of SMNPs, and thus, understanding the effects of geometry on LSPR properties for a SMNP is imperative work.

The optical properties of a SMNP can be tuned by controlling its topographic features, including the overall shape, edges and vertices [11, 14, 15]. In general, the electric field can be significantly improved by including sharp corners in the nanostructures [11, 16, 17], a fact which motivated the studies on the optical properties of nanowires [16], triangular nanoplates [18], and nanocubes [19]. Previous theoretical work has predicted that the maximum electric field intensity occurs at the tips of prolate particles and the waists of oblate particles, which have potential applications in SERS [17, 20]. On the other hand, large electric field (E-field) enhancement also occurs when the two vertices of dimers [21, 22], or arrays of nanoparticles [20, 23], are close enough to each other, a phenomenon known as "particle coupling." As a result, the LSPR spectrum exhibits a blue-shift when the polarization direction of the incident light is perpendicular to the array axis and a red-shift when the polarization direction is parallel to the array axis [20]. However, further studies of the effect of vertex angles and the number of vertices of a single nanostructure on LSPR properties need to be undertaken.

In this article, the effect of vertex geometry on LSPR properties for single metal nanostructures is developed based on insights into the change in optical properties, sensing performance, and E-field enhancement of nanostructures. We consider effects of nanostructure geometry, such as vertex angle and number of vertices, on LSPR behavior. These geometric features can be realized by currently available nanofabrication techniques [24]. A series of nanoparticles (nanostars) with regularly varying geometries is utilized to systematically explore these effects. Nanostars have many typical nanostructure features (several vertices and regions of high specific area) which make them optimum candidates for this study. The finite-difference time-domain (FDTD) method is applied to simulate the E-field of the nanostructures. These results are then analyzed and discussed in light of known relevant phenomena, such as the lightning rod effect (the aggregation of free electrons at the vertices which results in significant E-field enhancement) and E-field coupling. Valuable guidelines for the design of nanostructures for sensing applications are then extracted from the results.

2. Methods

The optical properties of SMNPs depend strongly on their shape. For a metal oblate spheroid with a characteristic size much smaller than the incident light wavelength λ, Mie theory [25] and Gans theory [26, 27] present an analytical method to describe their optical properties. In this case, the extinction efficiency $\sigma_{ext}(\lambda)$ can be described as follows:

$$\sigma_{ext}(\lambda) = \frac{2\pi}{3\lambda} V \varepsilon_d \sum_j \frac{\left(1/P_j\right)\varepsilon_{mi}(\lambda)}{\left(\varepsilon_{mr}(\lambda) + \frac{1-P_j}{P_j}\varepsilon_d\right)^2 + \varepsilon_{mi}^2(\lambda)} \tag{1}$$

#118796 - $15.00 USD Received 26 Oct 2009; revised 3 Dec 2009; accepted 6 Dec 2009; published 6 Jan 2010

Here, ε_d and ε_m are the dielectric functions of the external environment and the metal nanoparticle, with the subscript r and i representing the real and imaginary components of ε_m . The extinction efficiency is related to the extrinsic parameter ε_d and intrinsic parameters such as dielectric material ε_m , and the volume V of a nanoparticle. The depolarization factor P describes the particle shape, and it comprises three components: P_X , P_Y , and P_Z , correlating to the three radii of curvature of the oblate spheroid. For a sphere, these radii are identical, $P_X = P_Y = P_Z = 1/3$; whereas for an acicular particle, $P_x \approx 0$ and $P_Y = P_Z = 1/2$. But for an arbitrary non-spherical and non-ellipsoid particle such as a nanostar with several acute vertices, the depolarization factor P cannot be found analytically. In place of an analytical solution, numerical methods have been developed including the discrete dipole approximation (DDA) method and the FDTD method.

The FDTD method [28] is well-suited for studying the LSPR properties of metal nanostructures with arbitrary shapes, as it is known to generate accurate results when used for this application. By comparing FDTD electrodynamics calculations and LSPR measurements, excellent agreement was obtained in our previous work [11] and other studies [3, 19]. The FDTD numerical method evaluates the interaction of the applied electric field with the polarizable elements (electrons) in the time domain. The intensity of the electromagnetic field for an arbitrary spot in the space can be obtained by solving the transverse magnetic (TM) Maxwell curl equations and the transverse electric (TE) Maxwell curl equations in the difference form (i.e., the Yee equation) [29, 30]. Given the surface area of the nanoparticle, S, the extinction efficiency is obtained by:

$$\sigma_{ext}(\lambda) = \frac{P_{ext}(\lambda)}{P_{inc}(\lambda)} S \tag{2}$$

where the power transmission parameter P is obtained by the Poynting vector: $\vec{P} = \vec{E} \times \vec{H}$, with the subscripts ext and inc standing for the extinction power of emergent light and the power of incident light.

In our calculations, the material is assumed to be silver, with its complex relative dielectric constant ε_m obtained from Palik [31]. The illumination was performed under normal incidence and modeled as non-polarized in order to imitate natural light. To ensure the accuracy of computational results, a mesh override region is defined covering all of the vertices.

3. Dependence upon Vertex Angle

To investigate the effect of the vertex angle on LSPR performance, this work utilizes a series of silver delta-stars. Each delta-star can be described as shown in Fig. 1(a), depicted here as an equilateral triangle joined at its sides by three isosceles triangles. The outermost angles of these isosceles triangles are the vertices of the overall nanostructure. The vertex angle for each test case (nanostructure) ranges from α =15° to 60°, in increments of 5° and consistent for every angle of a single test case. Figure 1(c) presents three typical delta-stars: a three-needle-like star with each vertex angle of 15°, a typical delta-star of α =30°, and a triangular nanoplate with vertex angles of 60°.

#118796 - $15.00 USD Received 26 Oct 2009; revised 3 Dec 2009; accepted 6 Dec 2009; published 6 Jan 2010

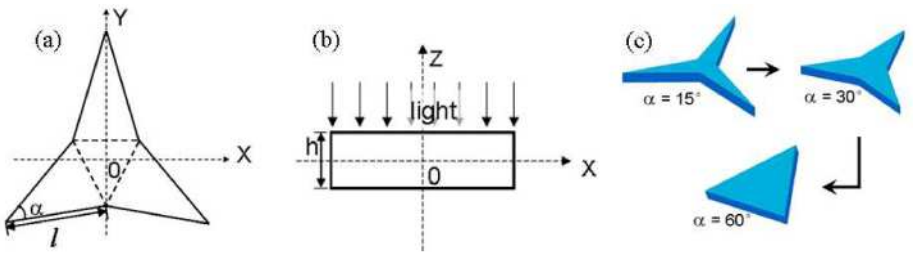

Fig. 1. The cross section in (a) X-Y direction and (b) X-Z direction of the simulated delta-star, and (c) three typical delta-stars with different vertex angles.

As Eq. (1) indicates, extinction efficiency is directly related to nanostructure volume. As such, the volume of each nanostructure is held constant at 209,000 nm^3. Each delta-star has a fixed height h of 50 nm (see Fig. 1(b)) and a surface area of 4180 nm^2. The surface area S is defined as: $S = \sqrt{3}l^2\left(\frac{\sqrt{3}}{2}\sin\alpha + \sin^2\frac{\alpha}{2}\right)$, which determines the edge length l by the vertex angle α. All the l values are listed in Table 1.

Table 1. Characteristic parameters of the delta-stars.

Vertex angle, α (°)	15°	20°	25°	30°	35°	40°	45°	50°	55°	60°
Length dimension, l (nm)	100	86	76.5	69.5	64.1	59.9	56.4	53.5	51.2	49.1

3.1 Optical Properties

Results indicate that an increase of the vertex angle α induces a blue-shift of dipole resonance and a strong decrease of extinction efficiency. When α =15°, the LSPR spectrum presents a dipole resonance peak at 991 nm and an extinction efficiency of 3.95%, as indicated in Fig. 2 (a). When α =30° the extinction spectrum has a peak wavelength λ^* of 704 nm, differing by 287 nm from that of α =15°. Also, the extinction efficiency is 3.25%, decreasing by 0.7%. Again, for the nanoparticle with α =60°, the dipole resonance peaks at 521nm, with an extinction efficiency of 1.53% (Fig. 2 (a)). In order to better resolve the overall relationship between the resonance wavelength and the vertex angles, we performed more calculations on different angles (15°–60° in 5° increments). The extinction spectrum peak wavelength λ^* as a function of vertex angle is plotted in Fig. 2 (b). As α increases from 15°to 60°, the decay of λ^* is initially rapid and then slows down, suggesting an exponential relationship.

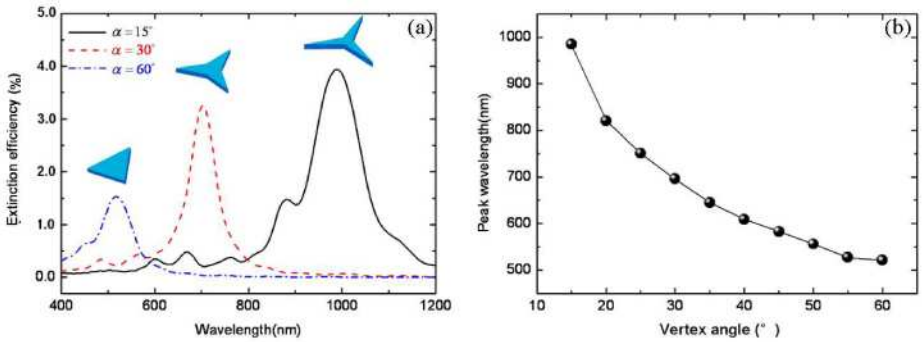

Fig. 2. (a) The plasmon resonance spectra for comparison of three different delta-stars. (b) The dipole resonance wavelength as a function of the vertex angle of the delta-stars.

#118796 - $15.00 USD Received 26 Oct 2009; revised 3 Dec 2009; accepted 6 Dec 2009; published 6 Jan 2010

The decays of resonant wavelength and the correlated decrease in extinction efficiency with the increasing vertex angle are a result of the aggregation of free electrons, also known as the lightning rod effect [16, 17]. The excitation of the electrostatic field by the free electrons is defined by: $E = \sigma / \varepsilon_0$, where ε_0 is the permittivity of the vacuum, and the electron areal density of charge σ describes the distribution of free electrons across the nanoparticle surface. Areal density σ is proportional to specific area, which is defined as $\eta = A/V$, where A is the surface area and V is the corresponding volume of a certain part of the nanostar. The much larger specific area η at the vertices than at other edges of the nanostar results in a much greater areal density σ of free electrons (Fig. 3(a)) and thus excites a much stronger electrostatic field (Fig. 3(b)).

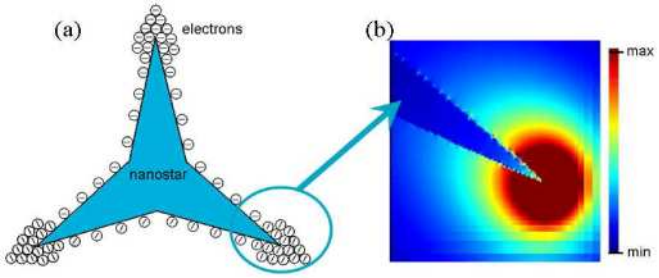

Fig. 3. Sketch of (a) free electron distribution and (b) the excited E-field around the vertex of a nanostar

When p-polarized (polarization direction parallel to X-axis in Fig. 1) incident light interacts with these free electrons, a quasi-static E-field is excited, and enhanced when the photon frequency is coincident with the localized surface plasmon resonance frequency. This effect is illustrated for two of the test cases in Fig. 4. Here we introduce a parameter, the "enhancement factor" (EF), which describes the E-field enhancement ability of a nanostructure. It can be defined as the ratio of excited E-field intensity and the incident E-field intensity. It is a function of the resonant wavelength λ^* , $EF\left(\lambda^*\right)$. In order to evaluate the E-field enhancement capability of single nanoparticles, we define a "maximal enhancement factor" (MEF) by $MEF = \max(\left|EF\left(\lambda^*\right)\right|^2)$. For the nanostar with a vertex angle of 15°, the MEF is approximately 2.3×10^4 at 991nm (Fig. 4(a)). The specific area at the vertices decreases sharply as the vertex angle increases, resulting in a much lower MEF. When α = 60°, the MEF = 2.44×10^3 at 521nm, approximately one tenth that of 15° (see Fig. 4(b)). This trend of the change in MEF with change of vertex angle is consistent with a previous study [16]. In addition, the vertex angle has significant influence on the localization of the excited E-field. Comparing Fig. 4(a) with Fig. 4(b), it is apparent that the E-field distribution near the vertices with α = 15° is more localized and intensified than that with α = 60°. It is the greater enhancement and more effective concentration of the E-field that contributes to the increase in extinction efficiency and red-shift in resonance wavelength of structures with vertices that are more acute.

#118796 - $15.00 USD Received 26 Oct 2009; revised 3 Dec 2009; accepted 6 Dec 2009; published 6 Jan 2010

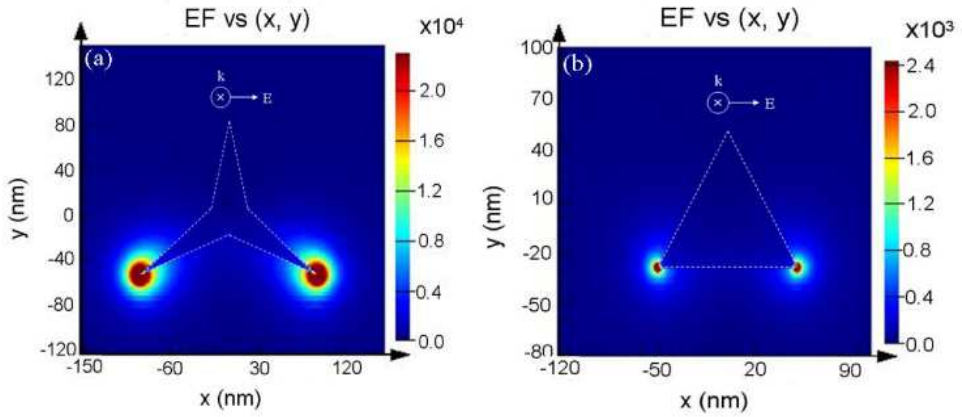

Fig. 4. Field enhancement of local E-fields of a delta-star with an angle of (a) 15° at 991nm and (b) 60° at 521nm

3.2. Sensing Performance

We now consider the possibility of exploiting these resonance spectra in biochemical sensing applications. With respect to Fig. 2 (a), it should be noted that for α = 15°, in addition to the dipole resonance, there is a quadrupole resonance peak at 881nm. This multi-pole resonance mode gives a wide *FWHM* (full-width at half-maximum) extinction spectrum of approximately 130nm. However, as listed in Table 2, the multi-pole resonance peak is modest for nanostars with larger vertex angles, and accordingly the *FWHM* is much narrower. Previous studies [18] have demonstrated that the acuteness of the vertices of a nanoparticle is important in determining the LSPR spectrum width: the more acute the vertices, the broader the spectrum width. A caveat to this assertion is that this will be true only for a nanoparticle with its vertices truncated at various lengths. The present results are consistent with the above expectations when vertex angles are smaller than 30°. However, for a nanostar with vertex angles larger than 30°, our FDTD calculations show that the LSPR spectrum width will become broader as α increases. The *FWHM* is an important parameter when evaluating the resolution factor for a single nanoparticle acting as a LSPR sensor, and its substantial variations in Table 2 play an important role in determining the figure of merit (*FOM*) of the LSPR sensor.

Table 2. The widths of plasmon resonance spectra, calculated peak positions sensitivity to dielectric environment, and the determined overall sensing performance for delta-stars with ten different vertex angles.

α (°)	15°	20°	25°	**30°**	35°	40°	45°	50°	55°	60°
FWHM (nm)	122	77	72	**66**	66	68	72	81	65	82
RIS (nm/RIU)	1108	717	678	**625**	579	526	499	447	438	427
FOM (RIU^{-1})	9.1	9.3	9.4	**9.5**	8.7	7.7	6.9	5.5	6.7	5.2

The figure of merit, which serves as a standard evaluation criterion for a single nanostructure acting as a LSPR sensor, is defined as $FOM = RIS / FWHM$, where *RIS* (refractive index sensitivity) denotes the peak wavelength λ^* shift per refractive index unit (RIU) change in ambient conditions. The *RIS* values listed in Table 2 show that smaller vertex angles result in higher refractive index sensitivities, and this relationship is almost identical to that between the resonant peak wavelength and vertex angle as shown in Fig. 2 (b). Recent theoretical work by Lazarides and associates [32] has suggested that the plasmon resonance spectral

#118796 - $15.00 USD Received 26 Oct 2009; revised 3 Dec 2009; accepted 6 Dec 2009; published 6 Jan 2010

position is the only parameter that determines the dielectric sensitivity of a single nanoparticle. Comparing the two parameters, *RIS* in Table 2 and λ^* in Fig. 2(b) as functions of the vertex angle α , our results are consistent with this hypothesis.

While the *RIS* is an important parameter, the *FOM* offers the best criterion for determining a trade-off between a narrow plasmon width and a high sensitivity, and is regarded as the most important parameter to assess the overall sensing performance of single nanostructures [18]. The *FOM* increases slowly as α increases from 15° to 30°, indicating that the sensing performance grows better as the vertices become less acute. However, when α increases from 30° to 60°, the sensing performance becomes increasingly poorer. These results provide qualitative insight into the relationship between sensing performance and the vertex angle of a nanostructure, and indicate that the optimum vertex angle is not an extreme but rather an intermediate value.

4. The Effect of the Number of Vertices on LSPR Sensing Performance

To evaluate the effect of the number of vertices of a nanostar on sensing performance the 30°-angle delta-star from Section 2 is used as a starting point and is extended to five new nanostars with increasing numbers of vertices: a cross star, a five pointed star, a hexangular star, a heptangular star, and an octangular star, as shown in Table 3. In each case the vertex angle is fixed at 30°; other detailed dimensions are described in Table 3.

In addition to the nanostars, another extreme case is the nanodisk, with a radius of 64.65 nm in the X-Y plane, which can be regarded as having an infinite number of vertices. The extinction spectra for the above seven types of nanostructures are presented in Fig. 5 (a), and a strong dependence on the number of vertex angles can be observed. In Fig. 5 (b) the peak shifts relative to the resonant peak of the nanostars are plotted versus the number of vertices. This plot indicates that the resonant peaks shift rapidly at first and then more gradually as the number of vertices increases, suggesting an exponential relationship between the number of vertices and the wavelength of the resonant peak. In addition, the change from three to eight vertices is sufficient to modify the spectral response, resulting in both a broadening of bandwidth and a decay of extinction efficiency (Fig. 5 (a)). This can be interpreted in term of the interaction between the surface charges at the neighboring tips, which qualitatively demonstrates tip-to-tip E-field coupling in the nanostructures.

Tip-to-tip coupling primarily occurs when the vertices of the nanostructure are in close proximity. The excited E-field enhancement factor (EF) distributions of resonant wavelength under p-polarized light for a delta-star and an octagonal star are shown in Fig. 6 (a) and Fig. 6 (b). Unlike Fig. 4, the EF distributions are plotted on a logarithmic scale instead of linear scale to give a clearer picture of tip-to-tip coupling. In the case of the delta star, the E-fields at the bottom two tips are largely isolated, while those for the octagonal star overlap, indicating that they interact with each other. This interaction plays a larger role than the E-field enhancement factor in determining the optical characteristics of the nanostructures, the result of which is that the octagonal star exhibits a shorter resonant wavelength and lower extinction efficiency despite the fact that it has a much bigger E-field MEF than the delta-star. The resonant peaks extracted from Fig. 5 (a) are plotted in Fig. 6 (c), where the tip-to-tip distance *d* (i.e., the distance between two vertices) becomes larger as the number of vertices decreases (Table 3). The large red shift as *d* increases gives a much clearer picture of the E-field coupling effect between vertices for single nanoparticles. This result resembles the near-field dipolar coupling between dimers [33, 34] under s-polarized light.

#118796 - $15.00 USD Received 26 Oct 2009; revised 3 Dec 2009; accepted 6 Dec 2009; published 6 Jan 2010

Table 3. the nanostar geometries and their characteristic parameters

Nanostructure Geometry	Particle dimension (nm)	Angle dimension (°)	Tip to tip distance (nm)	Surface area (nm^2)
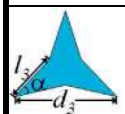 delta-star	l_3=69.48	α =30°	d_3=155	$S_3 = \sqrt{3}l_3^2\left(\frac{\sqrt{3}}{2}\sin\alpha + \sin^2\frac{\alpha}{2}\right) = 4180$
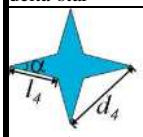 cross star	l_4=57.4	α =30°	d_4=99.45	$S_4 = 2l_4^2\left(\sin\beta + \frac{2\sin^2\frac{\beta}{2}}{\tan 45^\circ}\right) = 4180$
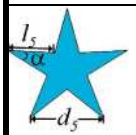 five pointed star	l_5=49.43	α =30°	d_5=76.82	$S_5 = 5l_5^2\left(\frac{1}{2}\sin\beta + \frac{\sin^2\frac{\beta}{2}}{\tan 36^\circ}\right) = 4180$
 hexangular star	l_6=43.63	α =30°	d_6=61.7	$S_6 = 3l_6^2\left(\sin\beta + 2\sqrt{3}\sin^2\frac{\beta}{2}\right) = 4180$
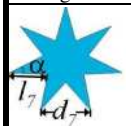 heptangular star	l_7=39.17	α =30°	d_7=51.06	$S_7 = 7l_7^2\left(\frac{1}{2}\sin\beta + \frac{\sin^2\frac{\beta}{2}}{\tan\frac{180^\circ}{7}}\right) = 4180$
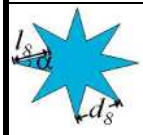 octangular star	l_8=35.62	α =30°	d_8=43.37	$S_8 = 4l_8^2\left(\sin\beta + \frac{2\sin^2\frac{\beta}{2}}{\tan 22.5^\circ}\right) = 4180$

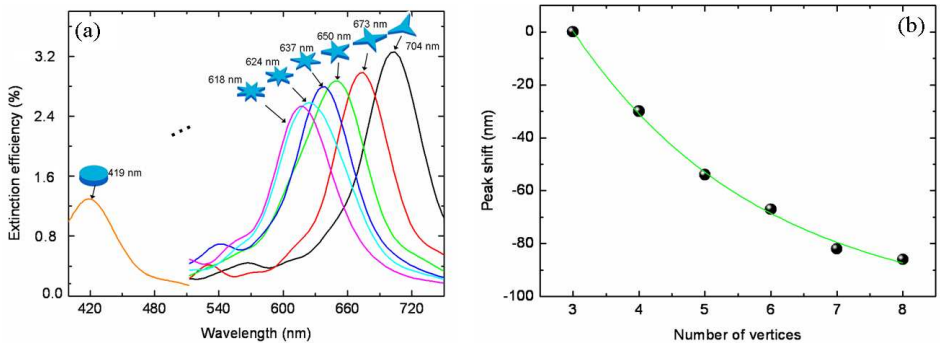

Fig. 5. (a) Extinction spectra of silver nanostructures with different numbers of vertices and (b) the relative peak shift as a function of the number of vertices for the nanostars.

#118796 - $15.00 USD Received 26 Oct 2009; revised 3 Dec 2009; accepted 6 Dec 2009; published 6 Jan 2010

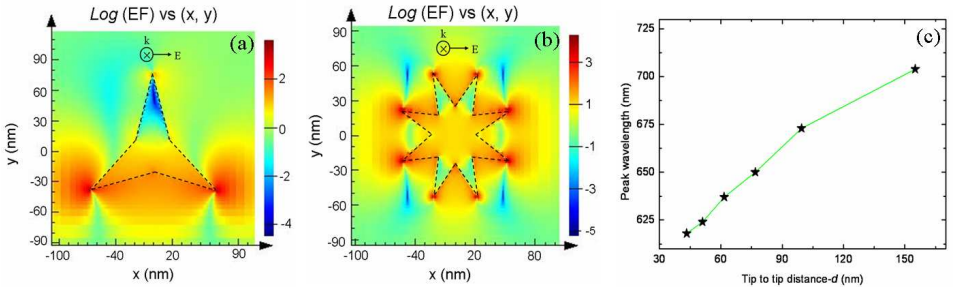

Fig. 6. The excited E-field distributions of (a) delta-star at 704 nm and (b) octagonal star at 618 nm and (c) the peak wavelength as a function of tip to tip distance *d* for nanostars.

In order to evaluate the sensing ability of single nanostars, the calculation of the extinction spectra is repeated when they are immersed in different dielectric environments with different refractive indices, and the obtained *RIS* values are listed in Table 4. Compared to the nanostars with a greater number of vertices, stars with fewer vertices show a much higher sensitivity to variations of dielectric environment. It also should be noted that for *FWHM* in Table 4, although generally the values become larger, they also vary greatly as the number of vertices increases. This is mainly attributed to the multi-pole resonance of five-pointed stars and heptangular stars. As a result, the *FOM* of target nanoparticles as a function of the number of vertices replotted in Fig. 7 exhibit some small variations from the predicted relationship of the first order exponential fitting line.

Table 4. The *FWHM*, *RIS*, and the determined *FOM* distributions of six different nanostars.

Angle amount	**3**	4	5	6	7	8
FWHM (nm)	**66**	67	82	70	80	70
RIS(nm/RIU)	**625**	604	562	542	504	491
FOM (RIU^{-1})	**9.5**	9.0	6.9	7.7	6.1	7.0

For the target nanostars, we find a *FOM* value of 9.5 for the delta-star (with 3 vertices) and 9.0 for the cross star (with 4 vertices) in Table 4, which is much higher than values previously reported for other nanostructure shapes [18, 19]. However, the sensing performance becomes poorer for other stars with more complicated geometry, resulting from the E-field coupling among the greater number of vertices. Thus, a nanostructure designer need not exploit complex structures to improve sensing performance.

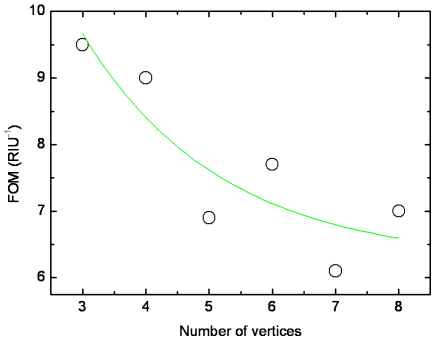

Fig. 7. Figure of merit distribution for nanostars with different numbers of vertices.

#118796 - $15.00 USD Received 26 Oct 2009; revised 3 Dec 2009; accepted 6 Dec 2009; published 6 Jan 2010

5. Conclusion

This paper presents a numerical study of the effect of the geometry of nanostructures on their optical properties and LSPR sensing performance. It is evident that the vertex features, including vertex angle and number of vertices, play an important role in determining the effectiveness of a nanostructure for use as a LSPR sensor.

A large blue shift is observed for the plasmon spectra of delta-stars under non-polarized light with a change in vertex angle from 15° to 60°. An exponential blue shift of peak wavelength and a decay of extinction efficiency are found to be based on the lightning rod effect. Compared with the triangular nanoplate (α = 60°), the MEF of the three-needle like star (α = 15°) is much bigger and the E-field distribution is much more localized. And in general, the overall sensing performance first improves with an increase in vertex angle, and then decreases beyond an optimum point of 30°.

In addition to the aggregation of free electrons at the vertices, the E-field coupling effect between neighboring vertices of a nanostructure is found to be important in determining the effectiveness of a single nanostructure in optical sensing. When vertices are fabricated closely together E-fields near the vertices interact with each other, resulting in a distinct blue shift of resonant wavelength as the number of vertices increases. A delta-star (with three vertices) exhibits a very high *FOM* of approximately 9.5, whereas other stars with more complicated geometry show much poorer sensing performance. These insights into the effects of vertex geometry on the optical properties and sensing performance of nanostructures can be used as guidelines in designing nanostructures for LSPR sensing.

Acknowledgements

This work has been supported by the Natural Science Foundation of China (60736037) and the Opening Project of Key Laboratory of Low Dimensional Quantum Structures and Quantum Control (Hunan Normal University), Ministry of Education, (QSQC0909).

#118796 - $15.00 USD Received 26 Oct 2009; revised 3 Dec 2009; accepted 6 Dec 2009; published 6 Jan 2010